THE PUBLISHING HOUSE
OF THE ROMANIAN ACADEMY

PROCEEDINGS OF THE ROMANIAN ACADEMY, Series A,
Volume 8, Number 1/2007, pp. 000–000

INFLUENCE OF THE BASAL ARBORIZATION ON THE FIRING PATTERN OF A BURST FIRING LAYER 5 NEOCORTICAL NEURON

Otilia PĂDURARU

Institute for Theoretical Computer Science, Romanian Academy, Iaşi branch
Blvd. Carol I, No. 8, Iaşi, 700505, Romania, E-mail: otilia@iit.iit.tuiasi.ro

Abstract. An important part of the neocortical layer 5 (L5) pyramidal cells are intrinsically burst firing neurons. To examine the influence of the basal arborization on the firing pattern of this cell type, computer simulations were run using a 'standard' model neuron and on four models obtained by altering the number or lengths of the basal trees arising from the soma. All models were endowed with 16 types of intrinsic active currents and complex Ca^{2+} dynamics. The simulations showed that the enlargement of the basal arborization leads to the diminution of the number of spikes/burst during the injection of a long current pulse, while its reduction has an opposite effect. Therefore, in the pyramidal cells of layer 5, the basal structure does not play an active role in the development of the depolarizing envelope underlying a burst.

Key words: burst firing neuron, multicompartmental modeling methods, basal arborization

1. INTRODUCTION

The neocortical L5 pyramidal cells are either regular spiking (RS) or intrinsically burst firing (IB) neurons [4], [14], reviewed in [2]. To a long current pulse of moderate amplitude, the IB cells fire repetitive bursts of action potentials (APs) whose strength (number of spikes/burst) may decrease in time. The diminution of burst strength in time is more prominent for stronger levels of depolarization [14]. On the contrary, the RS cells respond with a train of APs of decreasing frequency regardless of the depolarization level, as long as the external current is injected into the soma [4]. Both types of cells have similar basal arborization but differ in the morphology of the apical tree. The IB neurons have a long and thick apical trunk which ends in an extensive tuft while the apical trunk of the RS cells is thinner and gives rise to few distal branches [2].

The impact of the dendritic architecture on the electrophysiological response of the neocortical neurons has been the subject of several computational studies [6], [12], [9], [10]. Most studies have focused mainly on the influence of the apical morphology on the firing behavior of these cells. The goal of the present paper is to assess, by running computer simulations, whether the basal arborization plays an active role in the development of the depolarizing envelope underlying a burst in IB L5 neocortical neurons.

2. METHODS

The influence of the basal arborization on the firing pattern of an IB L5 neocortical neuron was examined in five model neurons using classical multicompartmental modeling methods and the NEURON simulation tool [3]. The soma-dendritic architecture of the 'standard' model (PyrL) was obtained from a neuron reconstructed by R. Douglas and coworkers [1], by elongating the apical trunk by 150 μm and by shortening the apical tuft by the same length. This modification was made since most L5 neocortical pyramidal neurons have long apical trunks [13] and, in addition, only this type of model neuron was able to reproduce the full range of experimental results recorded in IB L5 neocortical cells [8], [9]. The modified models were obtained from PyrL by removing one basal tree (PyrL –BT1), adding a new basal tree to the

original architecture (PyrL +BT11), shortening (PyrL 0.7 Bas) or elongating (PyrL 1.3 Bas) all basal dendrites by 30%. The original basal arborization consisted of 10 basal trees. BT1 (basal tree 1) consisted of 9 dendrites. The additional basal tree (BT11) had similar geometry and topology to BT1. A simplified axonal structure (not shown in Fig. 1), consisting of an axon hillock, an initial axonal segment, 5 nodes and 5 internodal myelin sheets (geometric parameters in [10]) was added to each soma-dendritic architecture. Each dendrite was longitudinally divided, when necessary, into several compartments so that the length of each compartment did not exceed 50 μm.

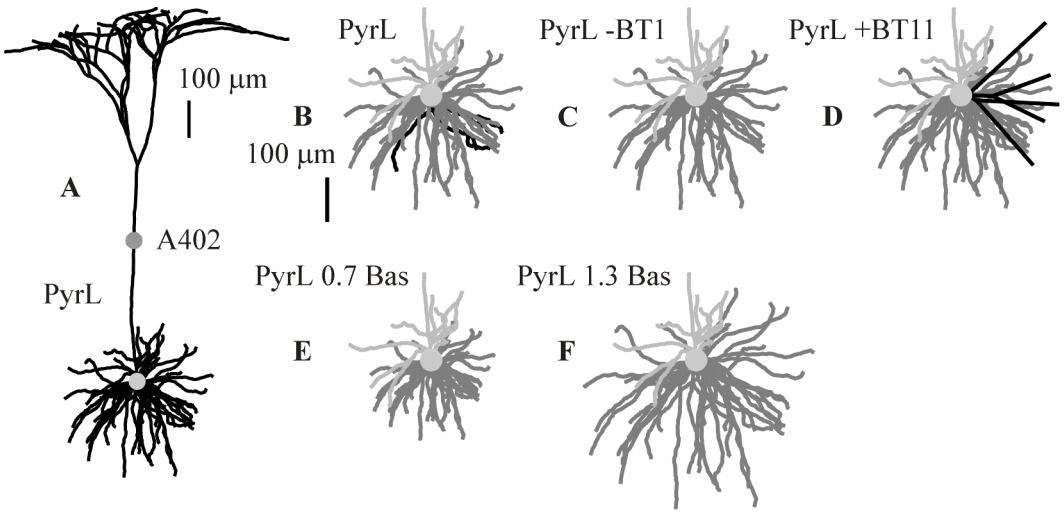

Fig. 1. Morphology of the soma-dendritic structure of the 'standard' model (PyrL) and of the lower part of all models. A. Soma-dendritic architecture of PyrL. The number following the character 'A' represents the distance (in μm) from the soma to the location marked by a dark gray circle. B-F. Shape of the lower part of PyrL (B), PyrL –BT1 (C), PyrL +BT11 (D), PyrL 0.7 Bas (E), PyrL 1.3 Bas (F). The visible fragment of the apical tree (including the proximal part of the apical trunk and the oblique dendrites arising from it) has been colored in light gray. The basal arborization has been colored in dark gray, except for the basal trees BT1 (in B) and BT11 (in D) which have been colored in black. In all figures, the soma is marked by a light gray circle. BT1 and BT11 are composed of 9 dendrites each, not all visible in B and D. Calibration in B also applies to C-F.

The specific membrane capacitance (C_m) was set to 0.04 μF/cm^2 (myelin sheets) [6] and 0.7 μF/cm^2 (elsewhere). The axial cytoplasmatic resistivity (R_i) was 70 Ωcm and the leak reversal potential (E_{leak}) was –65 mV, in all compartments. The values of the specific membrane resistance (R_m) followed a sigmoidal distribution along the dendritic paths [10], [13] with higher values (50000 Ωcm^2) near the soma and lower values (10000 Ωcm^2) at the distal apical sites. The specific leak conductance, g_{leak} was $1/R_m$ in all dendritic compartments. The soma and the axonal compartments had a g_{leak} value equal to $2 \cdot 10^{-5}$ S/cm^2 except for the nodes, where g_{leak} was 0.02 S/cm^2 [6]. Dendritic spines were taken into account by multiplying the specific membrane capacitances, leak and active conductances and permeabilities by 1.92 in all compartments, except for the somatic and axonal ones and those within the first 100 μm of the apical tree and the first 20 μm of the basal arborization, measured from the soma [5], [13]. For each compartment *j*, the variation of the membrane potential (v_j) was evaluated according to eq. 1,

$$A_j C_{m,j} \frac{dv_j}{dt} + A_j g_{leak,j} \left(v_j - E_{leak}\right) + A_j \sum_x I_x^{(j)} = I_{inj}^{(j)} + \sum_{k=1}^{N_j} \frac{v_k - v_j}{r_{k,j}} \quad (1)$$

where A_j is the area of the compartment, $C_{m,j}$ and $g_{leak,j}$ are the specific membrane capacitance and leak conductance respectively, E_{leak} is the leak reversal potential, the third left-hand side term is the sum of all *x*-type species of membrane voltage- and/or calcium-activated ionic currents present in this compartment, the second right-hand side term is the sum of all N_j axial currents entering or leaving compartment *j*, $r_{k,j}$ is the coupling resistance between compartments *j* and *k*, and $I_{inj}^{(j)}$ is an externally applied current, present only in the soma or in the compartment containing A402.

One or more of the following ionic current types were inserted into each compartment: a fast Na^+ current (I_{Na}), a fast delayed rectifier K^+ current (I_K), a persistent Na^+ current (I_{NaP}), five types of high voltage-activated (HVA) Ca^{2+} currents (I_L, I_N, I_P, I_Q, I_R) a low voltage-activated Ca^{2+} current (I_T), a transient, depolarization-activated K^+ current (I_A), a muscarinic type K^+ current (I_M), a slow K^+ current (I_{Ks}), an apamin-sensitive, Ca^{2+}-activated K^+ current (I_{mAHP}), a slow, apamin-insensitive, Ca^{2+}-activated K^+ current (I_{sAHP}), a voltage- and Ca^{2+}-dependent K^+ current (I_C) and a hyperpolarization-activated cation current (I_h). The Ca^{2+} currents were modeled by Goldman-Hodgkin-Katz equations (eq. 2), while the rest of the currents, except for I_C, were modeled by classical Hodgkin-Huxley type equations (eq. 3). All currents were expressed in mA/cm^2. The gating term ($m_x^{N1}h_x^{N2}$) represents the fraction of the *x*-type ionic channels in the 'open' state

$$I_x = \bar{p}_x m_x^{N1} h_x^{N2} \cdot \frac{z^2F^2v}{RT} \cdot \frac{\left[Ca^{2+}\right]_i - \left[Ca^{2+}\right]_o e^{\frac{-zFv}{RT}}}{1 - e^{\frac{-zFv}{RT}}} \tag{2}$$

$$I_x = \bar{g}_x m_x^{N1} h_x^{N2} \left(v - E_x\right) \tag{3}$$

In the equations above, $\bar{g}_x$, $\bar{p}_x$ and E_x are respectively the maximal specific conductance (S/cm^2), the maximal specific permeability (cm/s) and the Nernst reversal potential associated with the *x* type, z=2 is the Ca^{2+} valence, $[Ca^{2+}]_o$ = 2 mM is the external concentration of the Ca^{2+} ions, $[Ca^{2+}]_i$ is the internal concentration of the free Ca^{2+} ions in a thin shell below the membrane surface, T is the temperature in ^oK, R=8.314 joule·$^oK^{-1}$·$mole^{-1}$ is the gas constant, F=96485 coulomb/mole is Faraday's constant, m_x and h_x are the activation and inactivation variables respectively, obeying first-order kinetics with voltage– and/or $[Ca^{2+}]_i$– dependent steady-state and time constant functions and N1 (≤4) and N2 (0 or 1) are integers. The I_C type currents were modeled by an equation similar to eq. 3, except for the gating term, which was replaced by a variable whose values were computed from a kinetic scheme. The complete description of the 16 types of currents mentioned above can be found in the references included in [10].

In all neurons, the maximal specific conductances and permeabilities associated with these currents were distributed according to the same pattern. In what follows, 'val1(len1) → val2(len2)' will signify that the variable of interest – $\bar{g}_x$ (S/cm^2) or $\bar{p}_x$ (cm/s)– varies linearly from *val1* to *val2* between two points lying at distances equal to *len1* μm and *len2* μm from the soma. All distances were computed along the dendritic paths. For the basal arborization, the following pattern of distribution was used: $\bar{g}_{Na}$: 0.03(0) → 0(L_B), $\bar{g}_K$: 0.005(0) → 0(L_B), $\bar{g}_{NaP}$: $3\cdot10^{-4}$ (0) → 0(L_B), $\bar{p}_P$: $3\cdot10^{-5}$(0) → $3\cdot10^{-5}$(130) → 0(L_B), $\bar{p}_Q$: $5\cdot10^{-5}$(0) → $5\cdot10^{-5}$(130) → 0(L_B), $\bar{g}_A$: $3\cdot10^{-4}$(0) → 0(L_B), $\bar{g}_M$: $4\cdot10^{-4}$(0) → 0(L_B), $\bar{g}_{mAHP}$: $5\cdot10^{-5}$(0) → $5\cdot10^{-5}$(L_B), $\bar{g}_{sAHP}$: 10^{-4}(0) → 10^{-4}(L_B), $\bar{g}_C$: 0.01(0) → 0.01(L_B), where L_B stands for the length of the longest basal path and was equal to 304 μm (PyrL, PyrL –BT1, PyrL + BT11), 212.8 μm (PyrL 0.7 Bas) and 395.2 μm (PyrL 1.3 Bas). For the rest of the neuronal structures, $\bar{g}_x$ and $\bar{p}_x$ were distributed as described in [10]. Only 10 active current types were present in the basal arborization. Most active current types (15) were present in the apical tree. Based on the experimental results from [11], specific HVA Ca^{2+} channels were coupled to specific Ca^{2+}-dependent K^+ channels. This was accomplished by inserting only certain Ca^{2+} permeabilities and certain Ca^{2+}-dependent K^+ conductances into each compartment. Details about these associations can be found in [10].

The soma and each cylindrical dendritic compartment were radially divided into several concentric shells. Each shell had a thickness Δr equal to 0.2 μm, except for the outermost shell (shell 0) which was Δr/2 thick and the core [7]. For each compartment containing Ca^{2+} channels, the intracellular Ca^{2+} concentration was handled assuming that the Ca^{2+} ions bind to a global buffer [8], are pumped out by a Ca^{2+}-ATPase pump and a Na^+-Ca^{2+} exchanger [7] and diffuse radially across the cylindrical shells after entering the cell through Ca^{2+} channels [7]. Two additional leak Ca^{2+} fluxes were taken into account in the submembrane shell to compensate a significant decrease of $[Ca^{2+}]_i$ at rest [8]. All mechanisms modeling Ca^{2+} concentration (including Ca^{2+} influx [8]) were implemented by kinetic schemes. All parameters used to handle Ca^{2+} dynamics were given in [10]. The number of differential equations solved by each model exceeds 15000.

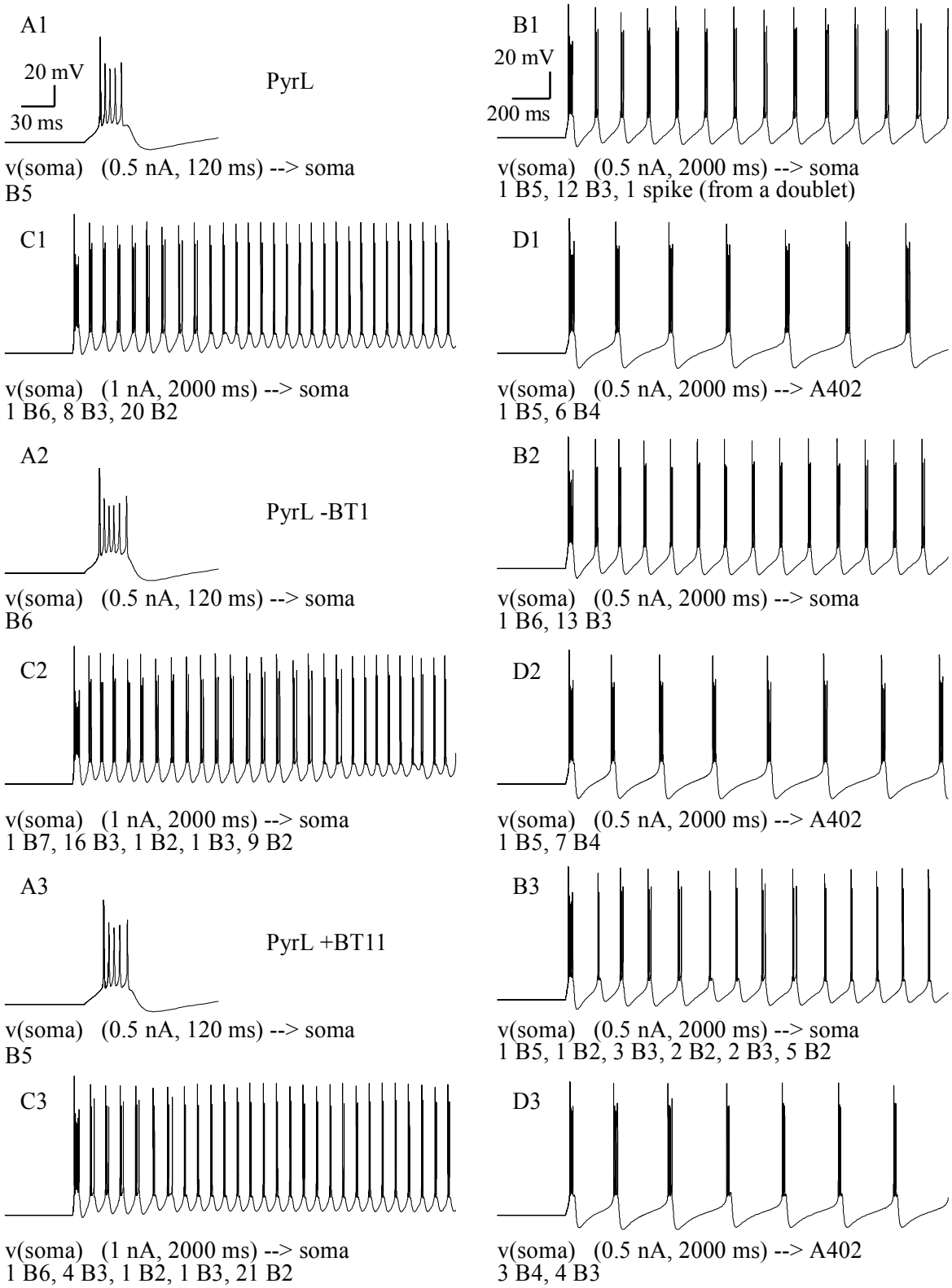

Fig. 2. Voltage responses of the PyrL (A1-D1), PyrL –BT1 (A2-D2) and PyrL +BT11 (A3-D3) models to current pulses injected either into the soma or into A402. The type of stimulation and the sequence of bursts, in alphanumeric format, are specified below each figure. Calibration in A1 also applies to A2 and A3. Calibration in B1 also applies to C1, D1, B2-D2, B3-D3.

3. RESULTS

The resting membrane potentials corresponding to the five models were equal to –63.89 mV (PyrL), -63.79 mV (PyrL –BT1), -64.05 mV (PyrL +BT11), -63.52 mV (PyrL 0.7 Bas), -64.27 mV (PyrL 1.3 Bas). PyrL 0.7 Bas had the smallest total area of the cell membrane, followed by PyrL –BT1, PyrL, PyrL +BT11 and PyrL 1.3 Bas. Each model neuron was stimulated by short (120 ms) or long (2000 ms) constant current pulses, injected either into the soma or into A402 (Fig. 1 A). The variation of the membrane potential was recorded only at the soma. In what follows, the pair '('x' nA, 'y' ms)', will refer to an 'x' nA current pulse applied for 'y' ms. The symbol 'Bn', where 'n' is an integer, will stand for an n-spike burst of APs. In each test, the external stimulus has been maintained until the end of the test.

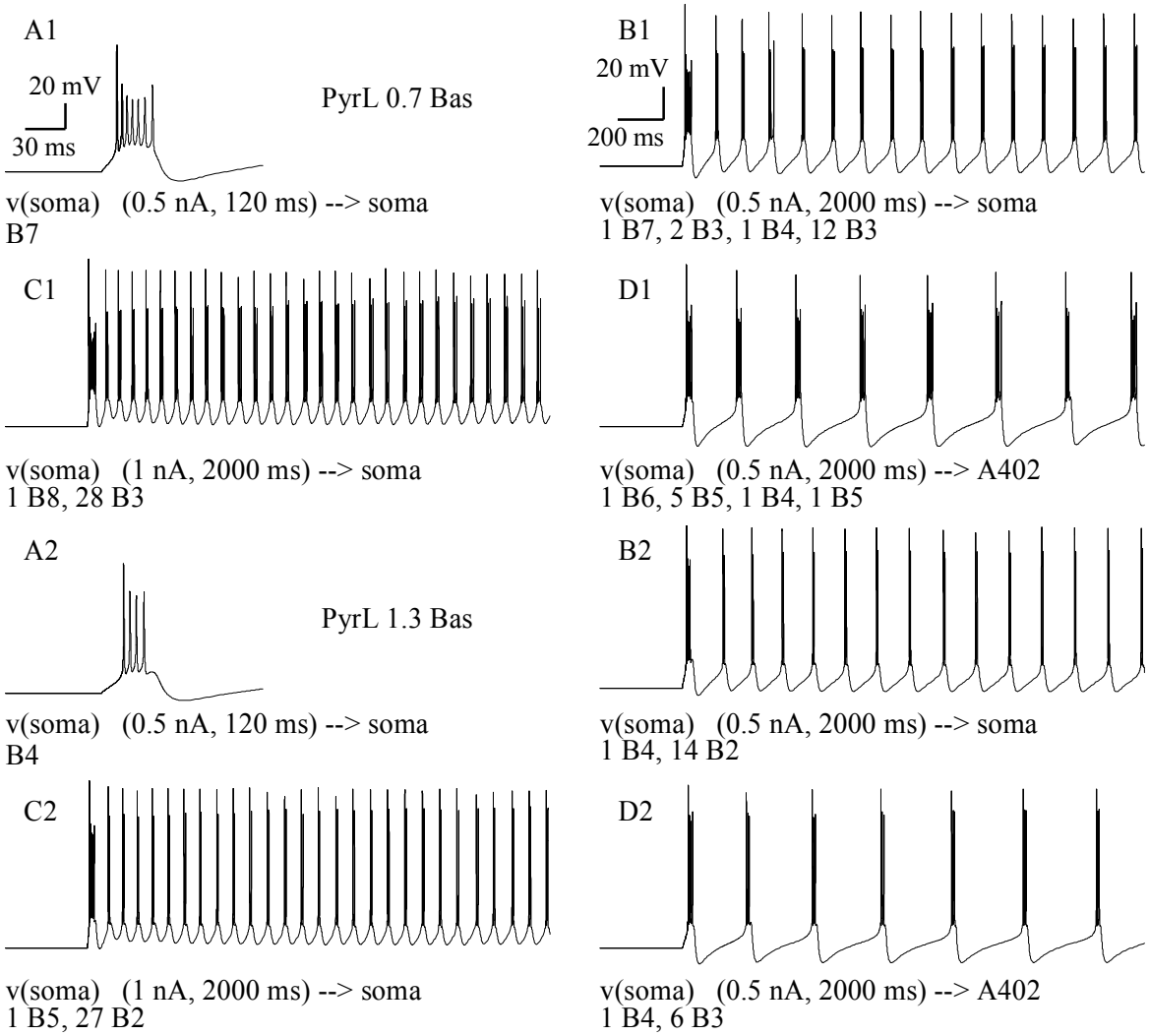

Fig. 3. Voltage responses of the PyrL 0.7 Bas (A1-D1) and PyrL 1.3 Bas (A2-D2) models to current pulses injected either into the soma or into A402. The type of stimulation and the sequence of bursts, in alphanumeric format, are specified below each figure. Calibration in A1 also applies to A2. Calibration in B1 also applies to C1, D1, B2-D2.

To a (0.5 nA, 120 ms) somatically injected current pulse, the models responded with B5 (PyrL), B6 (PyrL –BT1), B5 (PyrL +BT11), B7 (PyrL 0.7 Bas), B4 (PyrL 1.3 Bas). The responses to a (0.5 nA, 2000 ms) somatically injected current pulse were plotted in Fig. 2 B1 (PyrL), Fig. 2 B2 (PyrL –BT1), Fig. 2 B3 (PyrL +BT11), Fig. 3 B1 (PyrL 0.7 Bas), Fig 3 B2 (PyrL 1.3 Bas). The responses to a somatically injected (1 nA, 2000 ms) current pulse were plotted in Fig. 2 C1 (PyrL), Fig. 2 C2 (PyrL –BT1), Fig. 2 C3 (PyrL +BT11), Fig. 3 C1 (PyrL 0.7 Bas), Fig 3 C2 (PyrL 1.3 Bas). The responses to a (0.5 nA, 2000 ms) current pulse injected into A402 were plotted in Fig. 2 D1 (PyrL), Fig. 2 D2 (PyrL –BT1), Fig. 2 D3 (PyrL +BT11), Fig. 3 D1 (PyrL 0.7 Bas), Fig 3 D2 (PyrL 1.3 Bas). The type of stimulation and the sequence

of bursts, expressed in alphanumeric format, were specified below each plot. In Fig. 2 B1, the last spike evoked at the end of the 2000 ms stimulation was actually the first spike from a doublet which would have been completely developed if the stimulation had continued.

4. CONCLUSIONS

All model neurons examined in this study had the tendency to diminish the number of spikes/burst fired during the somatic injection of a long current pulse. This decrease in burst strength was faster for higher levels of depolarization. When a long current pulse was injected into a medial site of the apical trunk, each model responded with a sequence of stronger bursts comparing with the case when the same current was somatically injected. These results are in agreement to the experimental ones [14].

To the same stimulation, the decrease in burst strength during the somatic injection of a long current pulse was more prominent in a neuron with a larger basal area than in a neuron with a smaller basal area. In addition, a neuron with a larger basal arborization gave rise to weaker bursts during the injection of a long current pulse into the apical trunk than a neuron with a more restricted basal arborization, stimulated by the same current, at the same apical site.

Since the enlargement of the basal arborization led to the generation of weaker bursts during the injection of a long current pulse into the soma or into the apical trunk, it was concluded that the basal dendrites rather tend to impede than to contribute to the development of the depolarizing envelope underlying a burst.

REFERENCES

1. DOUGLAS, R., MARTIN K., WHITTERIDGE, D., *An intracellular analysis of the visual responses of neurones in cat visual cortex*, Journal of Physiology (London), **440**, 1, pp. 659–6962, 1991.
2. DOUGLAS, R., MARTIN K., *Neocortex*, In: *The Synaptic Organization of the Brain*, fourth edition, G. M. Shepherd (Editor), New York, Oxford University Press, pp. 459–509, 1998.
3. HINES, M.L., CARNEVALE, N.T., *The NEURON simulation environment*, Neural Computation, **9**, 6, pp. 1179–1209, 1997.
4. KIM, H.G., CONNORS, B.W., *Apical dendrites of the neocortex: correlation between sodium- and calcium-dependent spiking and pyramidal cell morphology*, Journal of Neuroscience **13**, 12, pp. 5201–5311, 1993.
5. LARKMAN, A.U., *Dendritic morphology of pyramidal neurones of the visual cortex of the rat. III. Spine distributions*, Journal of Comparative Neurology, **306**, 2, pp. 332–343, 1991.
6. MAINEN, Z.F., SEJNOWSKI, T.J., *Influence of dendritic structure on firing pattern in model neocortical neurons*, Nature, **382**, 6589, pp.363–366, 1996.
7. PĂDURARU, O., *Modeling Ca^{2+} transients in a burst firing neocortical layer V pyramidal neuron*, Memoriile Secţiilor Ştiinţifice ale Academiei Române, Series IV, tome XXV, pp. 249–270, 2002.
8. PĂDURARU, O., *Computer simulations on action potential initiation in intrinsically burst firing neocortical pyramidal neurons*, The Scientific Bulletin of the University of Piteşti. Electronics and Computer Science Series, **2**, pp. 82–93, 2003.
9. PĂDURARU, O., *The impact of the apical morphology of a layer V burst firing neocortical pyramidal cell on its discharge pattern*, The Scientific Bulletin of the Piteşti University, Series: Electronics and Computer Science, **2**, pp. 40–51, 2005.
10. PĂDURARU, O., *Propagation of subthreshold synaptic responses along the apical tree of a layer 5 burst firing neocortical neuron*, In: *Advances in Intelligent Systems and Technologies*, H. N. Teodorescu (Editor), Iaşi, Performantica Press,, pp. 49 – 66, 2006.
11. PINEDA, J.C., WATERS, R.S., FOEHRING, R.C., *Specificity in the interaction of HVA Ca^{2+} channel types with Ca^{2+}-dependent AHPs and firing behavior in neocortical pyramidal neurons*, Journal of Neurophysiology, **79**, 5, pp. 2522–2534, 1998.
12. SCHAEFER, A.T., LARKUM, M.E., SAKMANN, B., ROTH, A., *Coincidence detection in pyramidal neurons is tuned by their dendritic branching patterns*, Journal of Neurophysiology, **89**, 6, pp. 3143–3154, 2003.
13. STUART, G., SPRUSTON, N., *Determinants of voltage attenuation in neocortical pyramidal neuron dendrites*, Journal of Neuroscience, **18**, 10, pp. 3501–3510, 1998.
14. WILLIAMS, S.R., STUART, G.J., *Mechanisms and consequences of action potential burst firing in rat neocortical pyramidal neurons*, Journal of Physiology (London), **521**, 2, pp. 467–482, 1999.

Previous papers written by O. Păduraru can be downloaded from: http://iit.iit.tuiasi.ro/~otilia/Publications.html.

Received November 30, 2006